논 문

Evolution of Metastable $L1_2$-$Al_3(Nb_xZr_{1-x})$ Phases in Rapidly Quenched Al-Nb-Zr Alloys

Min-Woo Park†

Department of Materials Engineering, Kyungsung University 110, Daeyeon-dong, Busan, 608-736, Korea

Abstract

3원계 Al-Nb-Zr의 용융 합금을 스프렛 퀜칭(splat-quenching) 방법을 이용하여 급속냉각응고 한 후, 응고된 시편을 698K에서 200 시간까지 열처리하여 상전이를 연구하였다. 급속응고 및 열처리된 시편의 미세구조는 X-선 회절 및 투과전자현미경으로 분석하였다. Al-1.95Nb-0.65Zr, Al-1.3Nb-1.3Zr, 및 Al-0.65Nb-1.95Zr (at%) 3 원 합금계를 연구하였다. 각 합금의 조성은 Vegard's 법칙을 적용하여 Al(α) 의 기지조직과 $L1_2$-Al_3(Nb,Zr) 의 석출상들이 정합을 이루도록 선택되었다. 급속응고된 후 각 합금은 과고용된 Al(α) 의 고용상을 형성하였다. Al-1.3Nb-1.3Zr, 및 Al-0.65Nb-1.95Zr 의 급속응고된 상태의 시편을 698K 에서 열처리하여 알루미늄 기지와 정합의 계면을 갖는 $L1_2$-$Al_3(Nb_{0.5}Zr_{0.5})$ 와 $L1_2$-$Al_3(Nb_{0.25}Zr_{0.75})$ 의 상을 각각 석출하였다. 반면 Al-1.95Nb-0.65Zr 합금은 평형상인 $D0_{22}$-$Al_3(Nb_{0.75}Zr_{0.25})$ 상을 석출하였다. 준안정상의 정합 Al_3(Nb,Zr) 미세 분산상 석출은 입자의 조대화를 억제하고 재료의 고온 강도를 증가될 것으로 사료된다.

Key words : Al-Nb-Zr, Al_3Nb, Al_3Zr, Rapid-quenching, $L1_2$, Vegard's Law

(Received November 4, 2007 ; Accepted November 20, 2007)

1. Introduction

Binary Al alloys with the small addition of Nb, Ti, Zr, V, or Hf can precipitate Al_3M (M: transition metals) intermetallics of fine dispersoids in the Al matrix [1-6], which are stable at high temperature and highly resistant to coarsening. This is because these transition metals have very low solubility and diffusivity in Al(α) matrix, which can retard coarsening rate of the dispersoids [7]. The rate of coarsening can also be further reduced significantly by the formation of fine coherent precipitates in the Al(α) matrix [7]. However, the alloy processing by conventional casting method is very difficult due to the low solubility of transition metals in Al(α) matrix, as well as the large differences in melting temperature between Al(α) and transition metals. Either the rapid quenching or mechanical alloying has been used to process the supersaturated solid solution alloys at room temperature, followed by the anneal process to transforms to the fine dispersoids of Al_3M precipitates in the Al(α) matrix. For the Al-Nb alloy, the maximum solid solubility of Nb in Al(α) is very small (0.065 at%) and the diffusivity of Nb in Al(α) is very low [7]. Therefore, the Al-Nb is a promising, candidate alloy for the high temperature application.

The equilibrium phase of the Al_3Nb, Al_3Ti, and Al_3V is tetragonal $D0_{22}$, and the equilibrium phase of the Al_3Zr is tetragonal $D0_{23}$ structure [8,9]. However, except the Al_3Nb, these compounds can readily form the metastable phase of cubic $L1_2$-Al_3Ti, Al_3V and Al_3Zr before they finally transform to the equilibrium phase from the as-quenched state. The structure of Al(α) matrix is also cubic, thus the cubic $L1_2$ structure can have exact interfacial coherency with Al(α) matrix by the modification of the lattice parameter of the $L1_2$ phase.[10,11] By applying Vegard's law to the cubic $L1_2$ phase, the lattice parameter can be varied to match to the Al(α) matrix. For example, the lattice parameter of the $L1_2$-Al_3Ti, Al_3V and Al_3Zr structure can be varied by forming ternary compounds of the $L1_2$-$Al_3(V_xZr_{1-x})$ and $Al_3(Ti_xZr_{1-x})$ in the ternary alloys such as Al-V-Zr and Al-Ti-Zr alloys, respectively.

For the ternary Al-Nb-Zr alloy, it is of interest how to design the Al-Nb-Zr system and optimize the composition of added transition elements to minimize the lattice misfit between Al(α) matrix and $Al_3(Nb_xZr_{1-x})$ phase. Then it is important to understand which type of the $Al_3(Nb_xZr_{1-x})$ structure will be evolved from. The possible precipitated structure of the $Al_3(Nb_xZr_{1-x})$ could be the type of metastable $L1_2$-Al_3Zr, or either the type of stable $D0_{22}$-Al_3Nb or $D0_{23}$-Al_3Zr structure, which will be depending on the added composition of Nb and Zr. It is not excluded that the phases precipitated in the as-annealed specimen may be the

†E-mail : mwpark@ks.ac.kr

mixture of the $D0_{22}$, $D0_{23}$, and $L1_2$ structures. This is possible, if the Nb content in Al_3Zr exceeds the solubility limit or vice versa, the multiphase of $D0_{22}$, $D0_{23}$ and/or $L1_2$ Al_3M may precipitate.

It was reported that the metastable $L1_2$ phase of the Al_3Zr precipitate is stable and it does not transform to equilibrium $D0_{23}$ phase after annealing at 698K for 200 hours [12]. Thus, it is more probable that the Zr rich $Al_3(Nb_xZr_{1-x})$ phase would also precipitate as a $L1_2$ phase rather than the stable $D0_{23}$-Al_3Zr phase, however Nb rich $Al_3(Nb_xZr_{1-x})$ may precipitate as a $D0_{22}$ phase. Therefore, the Al-Nb-Zr alloys studied in this work is systematically designed to modify the lattice constant of the $L1_2$-Al_3Zr by varying the composition of Nb in $Al_3(Nb_xZr_{1-x})$ phase. It is also of interest to *investigate how the transformation of the* $Al_3(Nb_xZr_{1-x})$ phase will be evolved from the $L1_2$-Al_3Zr or $D0_{23}$ to $D0_{22}$-Al_3Nb, as the Nb composition in $Al_3(Nb_xZr_{1-x})$ increases.

2. Alloy Selection

It is based on the experimental results that the metastable $L1_2$ phase of the Al_3Zr precipitates do not transform to the equilibrium $D0_{23}$ phase after annealing at 698K for 200 hours. The alloy selection is then to minimize the lattice mismatch of the $L1_2$-$Al_3(Nb_xZr_{1-x})$ with the Al matrix by varying the composition of Nb and Zr. Thus, the alloy design in this work stems from the assumption that the precipitated structure of $Al_3(Nb_xZr_{1-x})$ is also the same cubic $L1_2$ phase of $L1_2$-Al_3Zr.

The lattice parameter of cubic $L1_2$-Al_3Zr is 0.4096 nm, whereas the lattice parameter of Al(α) at 698K is 0.40596 nm. Thus, the lattice parameter of cubic $L1_2$-Al_3Zr can be further reduced from 0.4096 to 0.40596 nm of Al(α) at 698K. The Vegard's law may be applied by considering the lattice parameters between the two crystals of $L1_2$-Al_3Zr and $L1_2$-Al_3Nb. However, it is not possible since the $L1_2$ phase formation of Al_3Nb has not been reported or is not possible.

It may be possible that the addition of Nb is soluble in $L1_2$-Al_3Zr, which can result in the formation of $L1_2$-$Al_3(Nb_xZr_{1-x})$ accompanying the variation of the lattice parameter. It is shown in Table 1 that the difference in lattice parameter between the equilibrium $D0_{22}$-Al_3Ti and $D0_{22}$-Al_3Nb phase is less than 0.1%. However, the metastable $L1_2$-Al_3Ti is 0.3967 nm as shown in Table 2. Thus, an assumption was made that the hypothetical $L1_2$-Al_3Nb has the same crystal structure and the lattice parameter of 0.3967 nm as that of $L1_2$-Al_3Ti. Then, the Vegard's law is applied between the two crystals of $L1_2$-Al_3Zr and $L1_2$-Al_3Nb.

Assuming the Vegard's law, the lattice parameter (denoted as a) of cubic $L1_2$-$Al_3(Nb_xZr_{1-x})$ will vary depending on the fraction of x, as analyzed in the following equation.

Table 1. Equilibrium phases and their lattice parameter of Al_3M compounds [13].

Compound	Structure	Lattice parameter(Å)
Al	cubic	a = 4.0562
Al_3Ti	$D0_{22}$	a = 3.849, c = 8.610
Al_3Nb	$D0_{22}$	a = 3.845, c = 8.601
Al_3V	$D0_{22}$	a = 3.780, c = 8.322
Al_3Zr	$D0_{23}$	a = 4.013, c = 17.321

Table 2. The lattice parameters of metastable cubic $L1_2$ structure of Al_3M [5].

Compound	Structure	Lattice parameter(Å)
Al	Cubic	a = 4.0596
Al_3Ti	$L1_2$	a = 3.967
Al_3Nb	unknown	assume(a = 3.967)
Al_3V	$L1_2$	a = 4.045
Al_3Zr	$L1_2$	a = 4.090

$$a\{L1_2\text{-}Al_3(Nb_xZr_{1-x})\} = 4.090Å(L1_2\text{-}Al_3Zr) - 0.123Å \times x$$

x is the fraction of Nb. 0.123Å is obtained from the calculation as shown below.

$$0.123Å = 4.090Å\{a(L1_2\text{-}Al_3Zr)\}\text{-}3.967Å\{a(L1_2\text{-}Al_3Ti)\}$$

The fraction of Nb, x, can be calculated to meet the condition that the lattice parameter a of Al is equal to a $[Al_3(Nb_xZr_{1-x})]$.

$$4.0596Å\{a(Al)\} = 4.090Å\ \{a(L1_2\text{-}Al_3Zr)]\} - 0.123Å \times x$$
$$\therefore x = 0.25$$

The simple calculation made above is based on the assumption. Thus, it is investigated how the lattice matching will be evolved from the experimental results. It is also studied how the metastable $L1_2$ phase may transit to the stable $D0_{22}$-Al_3Nb as the Nb addition increases.

3. Experimental

Al-Nb and Al-Nb-Zr alloys were prepared by using highly pure metals of Al(99.9%), Nb(99.8%), and Zr(99.9%). These metals were melted into alloy buttons on a Cu hearth by arc in an Ar atmosphere. The alloy buttons were then remelted more than 5 times. The compositions of the alloys studied in this work are listed in Table 3. The nominal compositions of the Al-1.5at% Nb alloy were chosen so that the volume of the Al_3Nb phase is 5.0%. However the nominal compositions of the Al-Nb-Zr alloys were chosen to have 10 volume(Vol.) % of the $Al_3(Nb_xZr_{1-x})$ phase. The differences

Table 3. Nominal compositions of Al-Nb-Zr Alloys.

Alloy	Nb (at%)	Zr (at%)
Al-Nb	1.5	-
Al-Nb-Zr	0.65	1.95
	1.3	1.3
	1.95	0.65

in Vol. % is to have less Nb content for the Al-Nb alloy: 1.5at% Nb for 5.0 Vol. % Al_3Nb; 3.13 at% Nb for 10 Vol.% Al_3Nb. The more the Nb is added in the Al-Nb, the higher the wetability of alloy on the Cu plate, which make rapid quenching difficult in the hammer and anvil method. However, the different Vol.% would not affect the phase evolution of the alloy, as far as the as-quenched state are supersaturated solid solution phase.

The alloy buttons were cut into many small pieces, which were then arc-melted and rapidly quenched by the hammer and anvil technique. The schematic of the hammer and anvil apparatus is shown in Figure 1. To study the precipitation of Al_3Nb and $Al_3(Nb_xZr_{1-x})$ phases, the as-quenched foils were heat treated at 698K for 200 hours in an Ar atmosphere.

The microstructures of the as-quenched and annealed alloy foils were studied by X-ray diffraction (X'Pert-MRD, Philips Co.). Transmission Electron Microscopy(TEM) using JEOL JEM 2010FX was also used to characterize the microstructures of the annealed specimens. The specimens for TEM studies were prepared by jet polishing at –40°C in a solution of 75% methanol and 25% nitric acid.

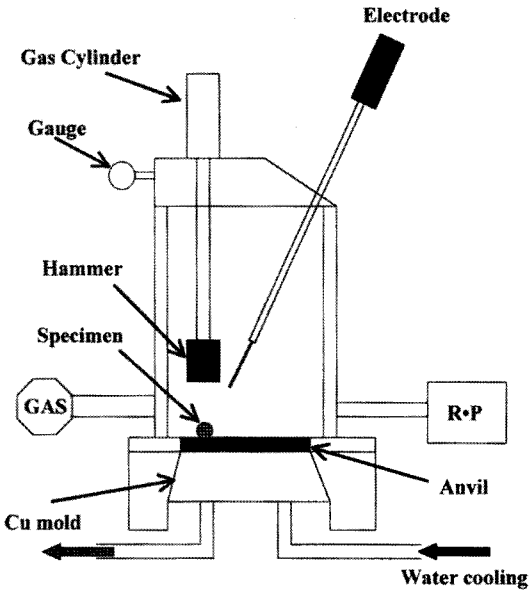

Fig. 1. Schematics of rapid quenching apparatus using hammer and anvil.

4. Results and Discussion

4.1 Microstructure of the as-quenched alloys

X-ray diffraction patterns obtained from the as-quenched Al-Nb and Al-Nb-Zr alloys are shown in Figure 2. The strong diffraction patterns from the FCC structure of Al(α) phase are shown for all the as-quenched alloys. No patterns from the other phases such as Al_3Nb and Al_3Zr are shown in Figure 2. Thus, it indicates that the as-quenched state of the alloys are the supersaturated Al(α) phase.

4.2 Phase evolution in the annealed alloys

Figure 3 shows X-ray diffraction patterns obtained from the annealed alloys at 698K for 200 hours. For the Al-1.5at.% Nb alloy, the strong patterns from the Al(α) (FCC) phase are observed, however there are few patterns from the other phases. The addition of 1.5 at.% Nb was chosen to yield only 5 Vol. % of Al_3Nb phase, thus it may be very difficult to get enough intensity over the background intensity.

For the ternary Al-Nb-Zr alloys, as it is shown in Figure

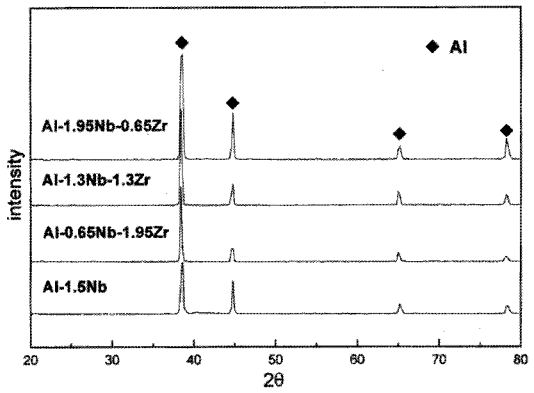

Fig. 2. X-ray diffraction patterns obtained from the as-quenched Al-Nb and Al-Nb-Zr alloys.

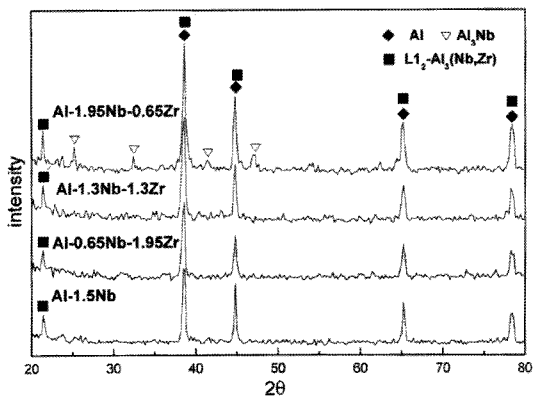

Fig. 3. X-ray diffraction patterns obtained from the annealed alloys at 698K for 200 hours.

3, the diffraction patterns from the stable $D0_{22}$-Al_3Nb is clearly shown in the Al-1.95Nb-0.65Zr alloy with the highest Nb content. As the Zr content increases for the Al-1.3Nb-1.3Zr and Al-0.65Nb-1.95Zr alloys, the patterns from the stable $D0_{22}$-Al_3Nb phase disappear, whereas the strong patterns from the Al(α) and $L1_2$-$Al_3(Nb_xZr_{1-x})$ are clearly shown.

Figure 4 shows the selected area electron diffraction pattern and the microstructure of the Al-0.65Nb-1.95Zr alloy annealed at 698K for 200 hours. The electron diffraction pattern clearly shows the superlattice patterns from the cubic $L1_2$-$Al_3(Nb_xZr_{1-x})$ phase. The superlattice patterns from the precipitates are very well matched to the stong Al(α) (FCC) patterns from the matrix.

Both the structures of Al(α) and $L1_2$-$Al_3(Nb_xZr_{1-x})$ are cubic, and the lattice parameters of both phases can be well matched as it was explained in the previous discussion of alloy selection. In the cubic $L1_2$-$Al_3(Nb_xZr_{1-x})$ structure, Al atoms are located at the center of six faces and the location of the either Nb or Zr atom is the eight corners of the cube.

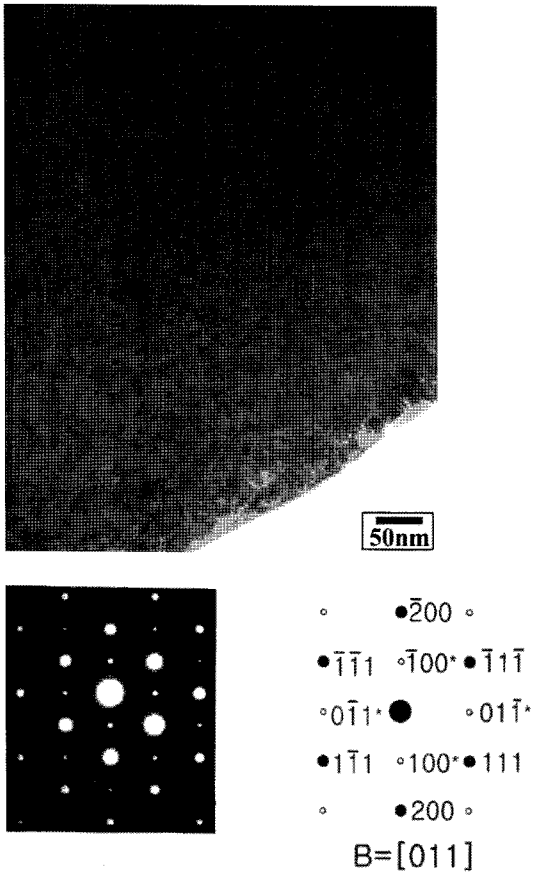

Fig. 4. Selected area electron diffraction pattern and the microstructure of the Al-0.65Nb-1.95Zr alloy annealed at 698K for 200 hours. *Diffraction patterns from the superlattice L12-Al3(NbxZr1-x) phase; ●Diffraction patterns from both the Al(a) and L12-Al3(NbxZr1-x) phases.

Thus, the mixed indices of (hkl)* planes in the $L1_2$-$Al_3(Nb_xZr_{1-x})$ phase provide weak superlattice patterns. In Table 4, the mixed indices of (hkl)* planes are listed with the 2θ values for the diffraction of $\lambda_{CuKa1} = 1.54056$Å.

Figure 5 shows the selected area electron diffraction pattern and the microstructure of the Al-1.3Nb-1.3Zr alloy annealed at 698K for 200 hours. The superlattice patterns from the precipitates are clearly shown in Figure 5, however the superlattice patterns are not well matched to

Table 4. The planes and d-spacings of the superlattice $L1_2$-$Al_3(Nb_xZr_{1-x})$ phase with the corresponding 2θ values ($\lambda_{CuKa1} = 1.54056$Å). *Diffraction planes of mixed indices from the superlattice $L1_2$-$Al_3(Nb_xZr_{1-x})$ phase.

Planes (hkl)	d-spacings (Å)	2θ(degree)
100*	4.0596	21.87
110*	2.8705	31.13
111	2.344	38.37
200	2.0298	44.60
210*	1.8155	50.21
211*	1.6573	55.39
220	1.4353	64.91

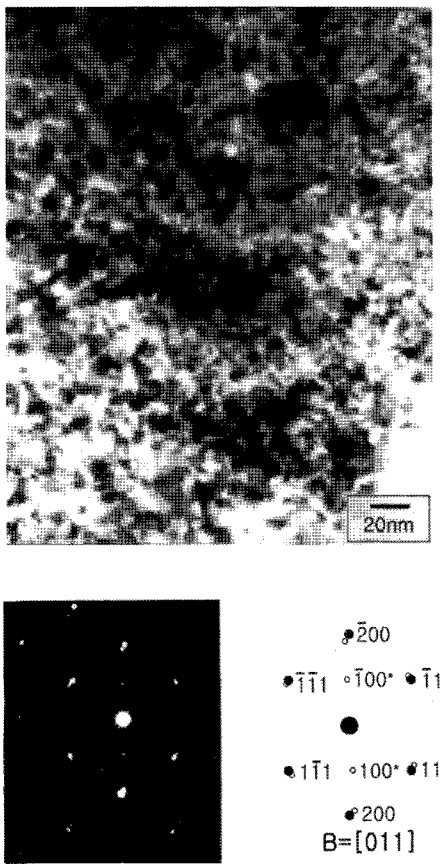

Fig. 5. Selected area electron diffraction pattern and the microstructure of the Al-1.3Nb-1.3Zr alloy annealed at 698K for 200 hours. *Diffraction patterns from the superlattice $L1_2$-$Al_3(Nb_xZr_{1-x})$ phase; ●Diffraction patterns from the Al(α) phase.

the stong Al(α) patterns from the matrix. It indicates that, although the $Al_3(Nb_xZr_{1-x})$ phase was precipitated as the metastable $L1_2$ phase in the Al-1.3Nb-1.3Zr alloy, the coherency of $L1_2$-$Al_3(Nb_xZr_{1-x})$ does not match well with the Al(α) matrix.

As it was discussed in the previous section of alloy selection, the ratio of Nb and Zr in the $Al_3(Nb_xZr_{1-x})$ phase was selected to yield $x = 0.5$ for the Al-1.3Nb-1.3Zr and $x = 0.25$ for the Al-0.65Nb-1.95Zr alloys. Calculation of $x = 0.25$ ratio was made so that the lattice parameter of $L1_2$-$Al_3(Nb_{0.25}Zr_{0.75})$ phase matches to the Al(α) matrix with 100% coherency, based on a simple assumption. It is clear now that both the Al-1.3Nb-1.3Zr and Al-0.65Nb-1.95Zr alloys result in precipitation of metastable cubic $L1_2$-$Al_3(Nb_xZr_{1-x})$ phase. However, the $L1_2$-$Al_3(Nb_{0.5}Zr_{0.5})$ phase in the Al-1.3Nb-1.3Zr alloy is less coherent than the $L1_2$-$Al_3(Nb_{0.25}Zr_{0.75})$ in the Al-0.65Nb-1.95Zr, as we have previously explained in section 2. The rate of coarsening can have the lowest value for the Al-0.65Nb-1.95Zr alloy since the formation of fine coherent precipitates in the Al(α) matrix.

5. Conclusion

An assumption was made that the hypothetical $L1_2$-Al_3Nb has the same crystal structure and the lattice parameter of 0.3967 nm as $L1_2$-Al_3Ti. The Vegard's law was applied between the two crystals of $L1_2$-Al_3Zr and $L1_2$-Al_3Nb. Then $x = 0.25$ ratio for the $L1_2$-$Al_3(Nb_xZr_{1-x})$ phase was calculated so that the lattice parameter of $L1_2$-$Al_3(Nb_{0.25}Zr_{0.75})$ phase matches to the Al(α) matrix with 100% coherency in the Al-0.65Nb-1.95Zr alloy.

The as-quenched states of all the Al-Nb-Zr alloys were the supersaturated Al(α) phase. As the Zr content increases for the Al-1.3Nb-1.3Zr and Al-0.65Nb-1.95Zr alloys from the Al-1.95Nb-0.65Zr alloy composition, the patterns from the metastable $L1_2$-$Al_3(Nb_xZr_{1-x})$ are clearly shown upon annealing at 698K for 200 hours. However, the patterns from the stable tetragonal $D0_{22}$-Al_3Nb phase disappear.

The $L1_2$-$Al_3(Nb_{0.5}Zr_{0.5})$ phase in the Al-1.3Nb-1.3Zr alloy is less coherent to the Al(α) matrix than the $L1_2$-$Al_3(Nb_{0.25}Zr_{0.75})$ phase in the Al-0.65Nb-1.95Zr. The rate of coarsening would be minimized for the Al-0.65Nb-1.95Zr alloy due to the increase of coherency of the fine $L1_2$-$Al_3(Nb_{0.25}Zr_{0.75})$ precipitates in the Al(α) matrix

Acknowledgments

This research was supported by the Kyungsung University Research Grant in 2005.

References

[1] D. K. Mukhopadhyay, C. Suryanarayana, and F. H. Froes, "Structural evolution in mechanically alloyed Al-Fe powders", Metall. Mat. Trans., 26A, (1995) pp. 1939-1946.

[2] H. Jones, "The status of rapid solidification of alloys in research and application", J. Mater. Sci., 19, (1984) p. 1043-1076.

[3] Y. C. Chen, M. E. Fine, and J. R. Weertman, "Microstructural evolution and mechanical properties of rapidly solidified aluminum-zirconium-vanadium alloys at high temperatures", Acta. Metall. Mater., 38, (1990) pp. 771-780.

[4] Y. C. Chen, M. E. Fine, J. R. Weertman, and R. E. Lewis, "Coarsening behavior of $L1_2$ structured $Al_3(Zr_xV_{1-x})$ precipitates in rapidly solidified aluminum-zirconium-vanadium alloy", Scripta. Metall., 21, (1987) pp. 1003-1008.

[5] S. Z. Han, S. C. Chung and H. M. Lee, Metall. "Alloy design and coarsening phenomenon of $L1_2$ precipitates in high-temperature Al-2 At. Pct (Ti,V,Zr) systems", Mat. Trans., 26A, (1995) pp. 1633-1639.

[6] A. A. Csontos and G. J.M Shiflet, "Chemistry and Physics of Nanostructures and Related Non-Equilibrium Materials", (eds., E. Ma et al), TMS, Warrendale, PA, (1977) p. 13.

[7] C. M. Adam, "Rapidly Solidified Amorphous and Crystalline Alloys", (eds., B. H. Kear, B. C. Giessen and M. Cohen), Elsevier Science Pub. Co. Inc., (1982) pp. 411-422.

[8] S. Tsunekawa and M. E. Fine, "Lattice parameters of aluminum-zirconium titanium ($Al_3Zr_xTi_{1-x}$) vs. x in aluminum-2 atomic % (titanium + zirconium) alloys", Scripta Metall., 16, (1982) pp. 391-392.

[9] M. S. Zedalis and M. E. Fine, "Lattice parameter variation of aluminum (titanium, vanadium, zirconium, hafnium) (Al_3(Ti, V, Zr, Hf)) in Al-2 atomic% (Ti,V,Zr,Hf) alloys" Scripta Metall., 17, (1983) pp. 1247-1251.

[10] M. S. Zedalis and M. E. Fine, "Precipitation and Ostwald ripening in dilute aluminum base-zirconium-vanadium alloys", Metall. Trans., 17A, (1986) pp. 2187-2198.

[11] N. Ryum, "Precipitation and recrystallization in an A1-0.5 WT.% Zr-alloy", Acta. Metall., 17, (1969) pp. 269-278.

[12] H. Lee, S. Z. Han, H. M. Lee, and Z. H. Lee, "Coarsening behavior of $L1_2$ precipitates in melt-spun aluminum-titanium-vanadium-zirconium alloys", Mater. Sci. Eng. A163, (1993) pp. 81-90.

[13] S. Z. Han, in Ph.D. Dissertation, KAIST, (1997) p.14.